Outstanding X-ray shielding effects of carbon nanotubes

Toshihiko Fujimori[1], Shuji Tsuruoka[1], Bunshi Fugetsu[2], Shigeo Maruyama[3], Akihiko Tanioka[4], M. Terrones[1,5], M.S. Dresselhaus[6], Morinobu Endo[1], Katsumi Kaneko[1]

[1]*Exotic Nanocarbon Research Center, Shinshu University, Wakasato 4-17-1, Nagano 380-8553, Japan*

[2]*Graduate School of Environmental Science, Hokkaido University, Sapporo, 060-0810 Japan*

[3]*Department of Mechanical Engineering, The University of Tokyo, 7-3-1 Hongo, Bunkyo-ku, Tokyo 133-8656, Japan*

[4]*Department of Organic and Polymeric Materials, Tokyo Institute of Technology, Meguro-ku, Tokyo 152-8552, Japan*

[5]*Department of Physics, Department of Materials Science and Engineering and Materials Research Institute. The Pennsylvania State University, 104 Davey Lab., University Park, Pennsylvania 16802, USA*

[6]*Deapartment of Physics and Materials Science, Massachusetts Institute of Technology, Cambridge, Massachusetts 02139-4307, USA*

[Abstract]

We report an outstanding phenomenon related to the X-ray attenuation induced by carbon nanotubes (CNTs). We observed that the mass attenuation coefficient of CNTs was significantly higher (> 100%) than that observed for highly oriented pyrolytic graphite (HOPG) and fullerenes (C_{60}). The attenuation coefficient of CNTs increased by reducing the sample thickness. This attenuation phenomenon could not be explained by the conventional particle theory or approximated wave equations, and an alternative theoretical explanation now needs to be formulated. In order to demonstrate the effect of CNTs, we coated a textile fabric with a thin film of CNTs and found an enhanced X-ray attenuation of 70%. Therefore, CNT materials could now be used in the fabrication of light-weight and efficient X-ray safety equipment and devices.

[Body]

Carbon nanotubes (CNTs) could exhibit a high degree of crystallinity and high electrical conductivity. The tubes could be mainly classified into single-walled carbon nanotubes (SWCNTs) and multi-walled carbon nanotubes (MWCNTs). Interestingly, these tubular structures have been used for electromagnetic shielding, particularly at high frequency in the GHz range. In this context, various types of CNT composites have been fabricated by mixing the tubes with resins (*1-3*) and ceramics (*4*). It is important to emphasize that CNTs possess a unique structure consisting of cylindrical tubules that could be nested (e.g. MWNTs), and the interaction of radiation with these tubules appears to be very different when compared to interactions with planar and stacked graphene sheets. The microwave energy absorption of CNTs is usually discussed in terms of the classic theory of Bethe-Bloch. The Peng's theoretical development (*5*), on the other hand, is based on Maxwell's equation, in which the electromagnetic absorption is attributed to collisions with hydrogen plasma that take place inside SWCNTs. The SWCNT contribution to the absorption has not been explicitly derived, and SWCNTs are usually considered as a conductive cylindrical vessel but its nanometer dimensions are not expressed in the developed equations. Although a clear explanation has not been provided, CNTs could convert microwave energy into light (*6*) and/or heat in high yields (*4*). These studies demonstrate that CNTs could exhibit outstanding electromagnetic effects.

The optical properties of CNTs are commonly studied based on the classic Maxwell-Garnett theory (*7*) and aligned CNTs (*8-10*) could be considered as the extreme dark material in addition to graphene. These authors demonstrate that the carbon surface of the densely packed CNTs perfectly absorbs with normal incidence to the tubular axis. In this context, Garcia-Vidal et al. (*8*) theoretically predicted that SWCNT arrays could absorb light efficiently. However, the hollow volumes (voids) and neighboring SWCNTs are not considered in the model since their contribution in the derived equation is not significant. In general, the light absorption of CNTs is usually explained by the surface environment of the array rather than the morphology of the CNT itself.

In this account, we report that CNTs could efficiently absorb X-rays when compared to highly oriented pyrolytic graphite (HOPG) (*11*). Interestingly, we have found that CNTs and CNT-coated fabrics efficiently absorb X-rays, and furthermore, their mass absorption coefficients could increase significantly by reducing the thickness of the specimens. These observations do not follow the classic laws of high energy photons.

Therefore, our results demonstrate that new models need to be reevaluated, especially when describing the interactions between photons and electrons within the solid crystal lattice.

In the classical physics framework, photon absorption passing through matter has been described using empirical equations. The well-known classic model of Beer-Lambert Law determines the photon absorbance as;

$$log_{10}\left(\frac{I}{I_0}\right) = -ax \tag{1}$$

or

$$\frac{I}{I_0} = \mathrm{e}^{-(\mu/\rho)\rho x} \tag{2}$$

where I, I_0, a, μ, ρ and x are, respectively, the transmitted intensity, the incident beam intensity, absorption coefficient, the linear absorption coefficient of material for X-ray absorption, the material density, and the distance that the photon travels through matter (the thickness of absorbing layer). The term (μ/ρ) is known as the mass attenuation coefficient and has been widely used as an intrinsic value in tables containing the X-ray mass attenuation coefficients (*11*).

It is noteworthy that effects related to photons passing through matter have been studied for years in the field of solid state physics. Compton (*12*) discussed the energy distribution and absorption using his theoretical development based on photon scattering. Subsequently, Wheeler and Lamb derived an approximation based on pair production (*13, 14*). Furthermore, the Born approximation is usually used to determine the contribution by the cross section of the material (*15*). Based on these seminal works, the energy profile of light incident into a solid uses the Bethe-Bloch equation (*16*). It is also important to note that an implicit agreement in all these studies, when dealing with particles passing through matter, considers Bravais lattices or periodic boundary conditions. However, one should also note that the carbon atoms in tubular and chiral concentric tubes are not periodic, and exhibit different degrees of curvature. Therefore, one could not use the HOPG model to explain effects of an incident photon in CNTs, and alternative approximations should be considered and developed.

Grüneis et al. (*17*) and Jiang et al. (*18*) have developed the theory related to the optical absorption of SWCNTs using band theory. They show an energy profile of CNTs, which

describes the absorption dependence based on the graphene chiral angle.

Sawada et al. proposed the Berry-phase transition in deformed crystals (*19*) and recent experimental results were carried out on large scale (*20*). These authors extend Bragg's law to the case of Si crystal deformation, and the Berry-phase transition is well described and has been supported experimentally (*20*). However, one should note that the large scale Berry-phase transition does not include changes in momentum of the light or the photon energy absorption. This suggests that there are missing terms that need to be used when studying CNTs and their curved surfaces.

In the present study, the X-ray attenuation using SWCNTs, MWCNTs, carbon nanohorns (SWCNHs), fullerenes (C_{60}), graphene oxide (GO), and a fabric-textile coated with MWCNTs were measured and compared with HOPG. MWNCTs from Mitsui Co. & Ltd. (MWNT-7) and SWCNTs prepared at the University of Tokyo were used. The SWCNHs sample was obtained from the NEC Corporation. Fullerenes were purchased from the Wako Chemical Co. The MWCNT-coated textile (C-Textile; 0.19 mm thick) was fabricated using polyester fibers coated with 8 wt% MWCNTs containing 2.5 wt% of TiO_2. Graphene oxide (GO) was prepared by the Hummers method. The X-ray absorption was measured in order to compare the difference between HOPG (stacked planar sheets) and cylindrical-tube carbon nanostructures. Samples other than HOPG, were compressed at 5×10^5 kN/m^2 in order to form a disc of 13 mm diameter; the thickness of the pellets depended on the samples used. SWCNHs were compressed at 3×10^5 kN/m^2. We used a monochromatic incident X-ray beam of MoK_α ($\lambda_0 = 0.7107$ Å, RINT TTR II, Rigaku) to irradiate all the samples mentioned above, so that the absorbance was measured. Figure 1 depicts a diagram explaining the orientation of the pellets with respect to the incident irradiation. Here, I_0 was the X-ray intensity measured without a sample. I and I_0 were averaged from 100 measurement points. The attenuation ratio and the mass attenuation coefficient were determined using Eq. (2).

Strikingly, a significant X-ray attenuation was observed when using CNTs and the textile coated with CNT (C-Textile) (see Figure 2). The mass attenuation coefficients of the SWCNTs, MWCNTs, SWCNHs, and the C-Textile are much larger than that of HOPG (0.576 to 0.581 cm^2/g) (*11, 21, 22*), which is depicted by the horizontal dot belt in Figure 2. Our measured mass attenuation coefficient in HOPG is very close to the value reported in the literature. It is noteworthy that the nanocarbons possessing cylindrical tube-like structures exhibit higher X-ray attenuation coefficient than that of

HOPG. In addition, the contribution of impurities was corrected using the table of the mass absorption coefficient (*11*). We also noted that the mass attenuation coefficient of fullerenes was almost equivalent with HOPG, and the cylindrically rolled graphene structures increase the X-ray attenuation significantly. This phenomenon does not follow any conventional model, since the mass attenuation coefficients should be determined by the nuclei within the material rather than by their crystal structures. Figure 3 shows the influence of sample thickness in the mass attenuation coefficients. MWCNTs show a clear dependence of mass attenuation coefficient on the thickness, whereas graphene oxides show a very mild dependence on the sample thickness. This observation confirms once more that graphene oxides (exhibiting a flat sheet structure) do not show any significant thickness dependence, but cylindrical carbon nanostructures do show such a dependence. It indicates that the cylindrical structure of carbon atoms causes the difference.

This unusually high attenuation property of MWCNTs could be efficiently transferred to the C-Textile (Figure 2). This C-Textile constitutes a semi-commercial product designed for planar heaters. However, we have found that this C-Textile has an alternative potential application consisting in the fabrication of X-ray shielding fabrics. The polyester filaments of C-Textile are uniformly coated by CNTs with a binder (Figure 4). Figure 5 shows the percentage attenuation vs. the thickness of the stacked textile sheets. The attenuation percentage rapidly increases by increasing the fabric thickness, reaching an absorption percentage higher than 70% with films 24 mm thick. Figure 6 shows X-ray transparency images and luminance distribution curves of the C-Textile and an aluminum plate obtained using a Shimadzu Microfocus X-Ray Testing System (SMX-1000). The aluminum plate (0.31 mm thick) is the most transparent against X-ray irradiation and reveals the sharp edges of the aluminum plate. However, the edges of both textiles, with and without MWCNTs, become diffused, indicating that both textiles are capable of attenuating X-ray more efficiently. The transparency difference between both textiles can be confirmed by evaluating the luminance distribution curves. Larger gray values indicate a higher transparency, and therefore the C-Textile is capable of shielding X-ray more efficiently than the textile without MWCNTs. For this reason, we believe that the C-Textile could be used as a main component in safety instruments and fabrics used for protection against X-ray radiation, and could be used in nuclear power plants and when operating medical equipment.

We have demonstrated the outstanding X-ray shielding of CNTs. The mechanism for these observations is far from clear and it cannot be understood by conventional particle

theory. The unusually high shielding effect of CNTs is likely to originate from their unique cylindrical nano-morphology. These observations are now opening new avenues for fabricating lightweight fabrics able to offer protection against X-ray radiation. However, further experimental and theoretical research is needed in order to elucidate the mechanism behind these reported observations.

Acknowledgement

We thank the Rigaku Co. for technical assistance and NEC Corpolation for complementally supplying us their SWCNHs. Also we thank Prof. Y. Natsume at Physics Department, Science school, Chiba University for his theoretical advice on solid physics. TF, ST, MT, ME and KK are supported by Exotic Nanocarbons, Japan Regional Innovation Strategy Program by the Excellence, JST.

References

1. Ye, Z, Deering W.D., Krokthin, A., Roberts, J.A. Microwave absorption by an array of carbon nanotubes: a phenomenological model. *Phys Rev B*; **74** (7) :075425 (2006).
2. Dudley, K.L. & Lawrence, R.W. Novel Carbon Nanotube-Polystyrene Foam Composites for Electromagnetic Interference Shielding, *Nano Lett* **5** (11) 2131-2134 (2005).
3. Liu, Z., Bai, G., Huang, Yi., Ma,Y., Du, F., Li, F., Guo, T., Chen, Y. Reflection and absorption contribution to the electromagnetic interference shielding of single-walled carbon nanotube/polyurethane composites *Carbon* **45** 821-827 (2007).
4. A.L. Higginbotham, P.G. Moloney, M.C. Waid, J.G. Duque, C. Kittrell, H.K. Schmidt, J.J. Stephenson, S. Arepalli, L.L. Yowell, J.M. Your, *Composite Science and technology* **68** 3087-3092 (2008).
5. Z. Peng, J. Peng, Y. Ou, *Phys Lett A* **359** 56-60 (2006).
6. T.J. Imholt, C.A. Dyke, B. Hasslacher, J.M. Perez, D.W. Proce, J.A. Roberts, J.B. Scott, A. Wadhawan, Z. Ye, J.M. Tour, J.M. *Chem Mater.* **15,** 3969-3970 (2003).
7. Maxwell-Garnett J.C. Colours in Metal Glasses and in Metallic Films. *Philosophical Transactions Series A*, **203** 385-420 (1904).
8. F.J. Garcia-Vidal, J.M. Pitarke, J.B. Pendry, *Phys Rev Lett* **78** (22) 4289-4292 (1997).
9. Z. Yang, L. Ci, J.A. Bur, S. Lin, P.M. Ajayan, *Nano Letters* **8** (2) 446-451 (2008).
10. K. Mizuno, J. Ishii, H. Kishida, Y. Hayamizu, S. Yasuda, D.N. Futaba, M. Yumura, K. Hata, PNAS, **106**, 15 (2009).
11. J.H. Hubbel S.M. Seltzer, *NIST Standard Reference Database* **126** (2004)
12. A.H. Compton, *Phys Rev* **21,** (5), 483 (1923).

13. J.A. Wheeler, W.E. Lamb, *Phys Rev* **55**, 858 (1939),
14. J.A. Wheeler, W.E. Lamb, *Phys Rev* **101 Erratta,** 1836 (1956).
15. Y.S. Tsai, *Rev Mod Phys* **46**, 815 (1974)
16. H. Bichsel, D.E. Groom, S.R. Klein, *PDG* Apr. (2006).
17. A. Grüneis, R. Saito, Ge. G. Samsonidze, T.Kimura, M.A. Pimenta, A. Jorio, A.G.Souza Filho, G. Dresselhaus, M.S. Dresselhaus, *Phys Rev B* **67**, 165402 (2003).
18. J. Jiang, R.Saito, A. Grünei, G.Dresselhaus, M.S. Dresselhaus, *Carbon* **42**, 3169-3176 (2004).
19. K. Sawada, S. Murakami, N. Nagaosa, *Phys Rev Lett* **96**, 154802 (2006).
20. Y. Kohmura, K. Sawada, T. Ishikawa, *Phys Rev Lett* **104**, 244801 (2010).
21. Handbook of X-ray diffraction, Rigaku Co. Ltd., (2010).
22. Chemical Society of Japan, "Kagaku Benran" (Handbook of Chemistry) "Kiso Hen II" (Fundamentals II), Maruzen Ltd., Tokyo (1984).

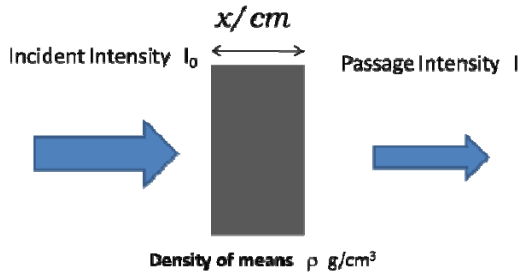

Figure 1. Schematic diagram used to measure different samples placed at the target holder of the X-ray equipment.

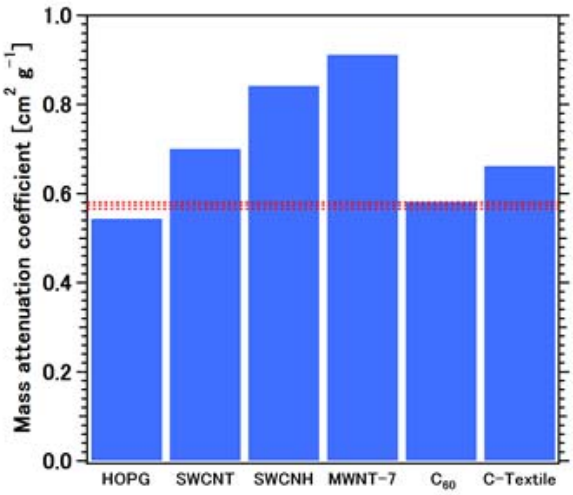

Figure 2. Mass attenuation coefficients of different carbon materials. The incident X-ray ray beam was monochromatic MoK_α (λ =0.7107 Å) at 50 kV and 10 mA. Width of the horizontal red belt shows the graphite mass attenuation coefficient in the literatures (*11, 21 and 22*); those attenuation coefficients for pure graphite are 0.566 (*22*), 0.576 (*21*) and 0.581 (*11*) $cm^2 g^{-1}$.

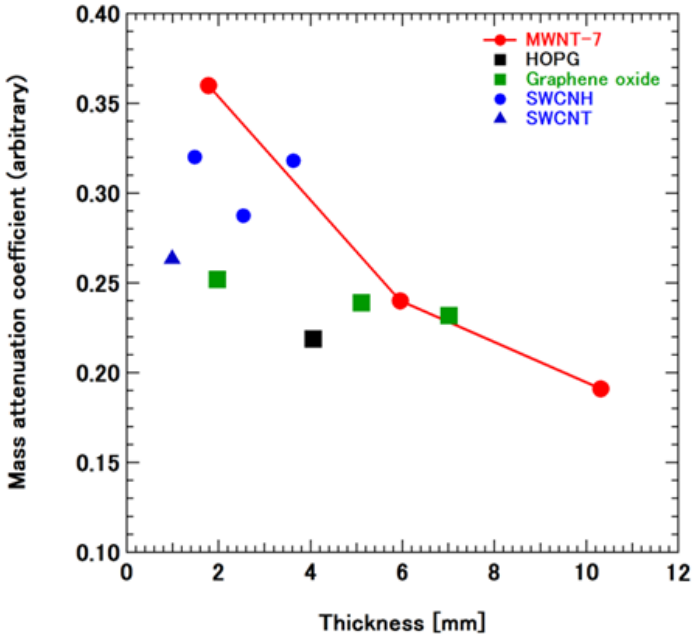

Figure 3. Mass attenuation coefficients of vrious nanostructured carbon materials of different thicknesses. The incident X-ray ray beam was non-monochromatic MoK$_\alpha$ (λ =0.7107 Å) at 50 kV and 300 mA (RINT TTR II, Rigaku). HOPG has a fixed value and graphene oxide changed slightly with the thickness.

(a) (b)

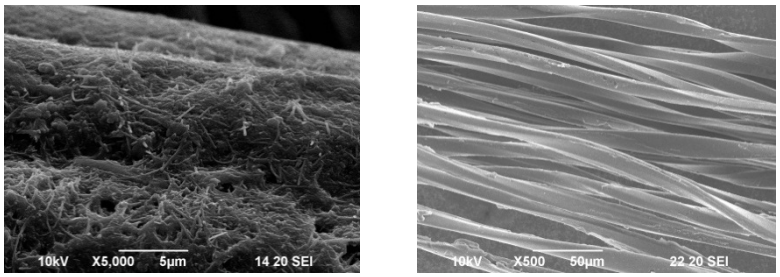

Figure 4. SEM images of: (a) the fabric filaments coated with CNTs; (b) lower magnification of the fabric showing the fiber yarns.

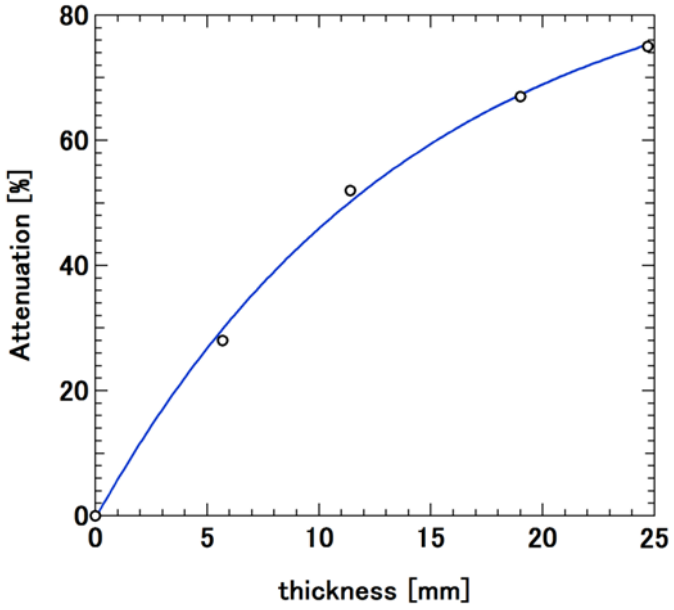

Figure 5. X-ray attenuation ratio as a function of the C-textile thickness. The incident X-ray of MoK_{α} was the same as the one shown in the previous measurements. An individual C-textile sheet exhibited a thickness of 0.19 mm, and the sample was made thicker by adding subsequent sheets of fabric.

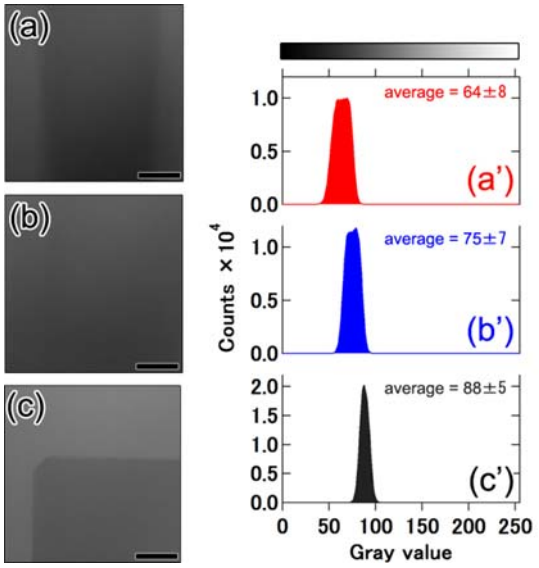

Figure 6. X-ray transparency images and luminance distribution curves using a Shimadzu Microfocus X-Ray Testing System (SMX-1000). (a) C-Textile coated with CNTs with a 3.8 mm thickness; (b) Textile without CNTs and with a 5.0 mm thickness, and (c) an aluminum plate with 0.31 mm thickness. The luminance distribution curves (a'), (b') and (c') correspond to (a), (b) and (c), respectively.